Catalysis Today 156 (2010) 246–253

Contents lists available at ScienceDirect

Catalysis Today

journal homepage: www.elsevier.com/locate/cattod

Influence of the oxygen feed distribution on the performance of a catalytic reactor for ATR of methane

M.L. Rodriguez [a], D.E. Ardissone [b], M.N. Pedernera [a], D.O. Borio [a,*]

[a] PLAPIQUI (UNS-CONICET), Camino La Carrindanga Km. 7, 8000 Bahía Blanca, Argentina
[b] FICES (UNSL), Av. 25 de Mayo 384, 5730 Villa Mercedes (San Luis), Argentina

ARTICLE INFO

Article history:
Received 24 July 2009
Received in revised form 13 April 2010
Accepted 20 April 2010
Available online 17 June 2010

Keywords:
Autothermal reforming
Membrane reactor
Oxygen feed distribution

ABSTRACT

In the present contribution, a theoretical study of a multitubular membrane reactor (MR) for the autothermal reforming of methane (ATR) over a $Ni/MgOAl_2O_3$ catalyst is presented.

By means of a pseudo-homogeneous 1D model, the viability and convenience of the proposed design to produce hydrogen to feed a PEM fuel cell of 10 kW_{th} is analyzed. The influence of the operating conditions on the reactor behavior is studied.

The results suggest that the MR is a promising alternative to conventional reactors to carry out ATR of methane at milder conditions and with similar H_2 productions. The axial distribution of the O_2 fed to the reactor is a powerful tool to influence the axial temperature profiles, the methane conversion and the selectivity. However, the reactor should be operated carefully, to avoid operating conditions where an accumulation phenomenon of oxygen along the axial axis appears.

1. Introduction

Fuel cells are devices capable of transform chemical energy in absence of combustion. Therefore, their theoretical efficiency is not limited by the difficulty of Carnot's cycle, as it happens in conventional plants of energy production or internal combustion engines.

PEM fuel cells need H_2 or a H_2 rich gas as fuel. Their most important advantages over other types of cells are high energy density, fast time of ignition and response, low operating temperatures and compact system. These characteristics made PEMFC suitable for automotive transport.

The inconveniences related with the distribution and storage of H_2 due to its low volumetric energy density at constant pressure and temperature, make necessary the production of H_2 *in situ* from other fuels, e. g., gasoline, natural gas, ethanol, etc.

There are two main processes to produce H_2 from hydrocarbons and alcohols: steam reforming (SR), and partial oxidation (POx).

Steam reforming of methane is the most important process for the production of H_2 and it has been widely investigated [1,2]. In this process, steam reacts with methane in presence of an appropriate catalyst to produce synthesis gas. Even though SR process can obtain high yields, the strong endothermicity of the reactions makes it necessary to provide a large amount of heat by fuel burning (commonly natural gas) in the furnace chamber. Because of this energetic demand, the reformer configuration becomes very large and impractical for fuel cells in mobile uses appliances.

To solve the problems associated to the heat transfer in steam reformers, partial oxidation (POx) has been used as an alternative method to produce H_2 or synthesis gas from methane [3]. This process is exothermic and presents a quick ignition even in absence of a catalyst. It can reach temperatures greater than 1000 °C, which allows an adiabatic operation and promotes the reforming of the remaining methane. However, partial oxidation leads to high carbon monoxide concentrations, which are undesirable for PEM fuel cells.

The autothermal reforming (ATR) combines the thermal effects of partial (or total) oxidation of methane and steam reforming reactions by means of the simultaneous feeding of methane, steam and air (or oxygen). Both processes occur simultaneously in the presence of a convenient catalyst. The energy generated from the oxidation reaction is used for SR, leading to diminishing local temperatures which favor the *Water Gas Shift Reaction* (WGSR). This reaction is slightly exothermic and consumes carbon monoxide to produce more H_2. The ATR reactor is then a compact system that is considered as an attractive alternative to mobile fuel cells [6].

However, a common problem in ATR reactors is the evolution of the axial temperature profiles, which can exhibit pronounced hot spots near the reactor inlet [3–5]. These high temperatures introduce considerable stress on the reactor materials and can damage the catalyst, particularly when a $Ni/MgOAl_2O_3$ catalyst is employed [6].

A possible alternative to reduce or eliminate the hot spots is the distribution of the oxygen feed along the reactor length [7–9]. This

* Corresponding author. Tel.: +54 291 4861700; fax: +54 291 4861600.
E-mail address: dborio@plapiqui.edu.ar (D.O. Borio).

0920-5861/$ – see front matter © 2010 Elsevier B.V. All rights reserved.
doi:10.1016/j.cattod.2010.04.023

Nomenclature

A_T	cross sectional area of tubes, m^2
B_0	geometric parameter, m^2
C_{pj}	specific heat of component j, kJ/(kmol K)
d_p	equivalent diameter of the catalyst pellet (momentum equation), m
d_S	shell diameter, m
d_T	internal tube diameter, m
D^e_{ij}	Effective molecular diffusion coefficient of component j, m^2/s
$D^e_{j,k}$	Effective Knudsen diffusion coefficient of component j, m^2/s
D^e_j	Bosanquet diffusion coefficient of component j, m^2/s
f	friction factor, dimensionless
F_j	molar flow of component j, kmol/h
F_{S_0}	feed flowrate of O_2 (shell side), Nm^3/h
F_{T_0}	total feed flowrate, Nm^3/h
J_j	permeation flow of component j, $kmol_j/(s\,m^2)$
$k_1{}^a$, $k_1{}^b$	kinetic constants of r_1, $kmol/(kg_{cat}\,s\,Pa^2)$
k_2	kinetic constant of r_2, $kmol\,Pa^{0.5}/(kg_{cat}\,s)$
k_3	kinetic constant of r_3, $kmol/(kg_{cat}\,s\,Pa)$
k_4	kinetic constant of r_4, $kmol\,Pa^{0.5}/(kg_{cat}\,s)$
K_0	geometric parameter, m
$K_{eq,2}$	equilibrium constants of r_2, Pa^2
$K_{eq,3}$	equilibrium constants of r_3, dimensionless
$K_{eq,4}$	equilibrium constants of r_4, Pa^2
K_j	adsorption constant for component j, Pa^{-1}
L	tube length, m
M_j	molecular weight of component j, kg/kmol
n_T	number of tubes
p_j	partial pressure of component j (tube side), Pa
P	total pressure, Pa
r_i	reaction rate of reaction i, $kmol_j/(kg_{cat}\,s)$
R	universal gas constant, $Pa\,m^3/(kmol\,K)$
R_f	oxygen feed ratio ($F^0_{O_2}/F^T_{O_2}$), dimensionless
S_G	global selectivity, dimensionless
T	temperature (tube side), K
T_m	average temperature, K
u_s	superficial velocity, $m_f{}^3/m_r{}^2\,s$
U	overall heat-transfer coefficient, $W/(m^2\,K)$
z	axial coordinate, m

Subscripts

S	shell side
0	at the axial coordinate $z=0$
L	at the axial coordinate $z=L$
i	reaction i
j	component j

Superscripts

T	Total
S	shell side
0	at the axial coordinate $z=0$
L	at the axial coordinate $z=L$
OX	combustion reaction

Greek letters

δ	membrane thickness, m
ΔH_{ri}	heat of reaction i, kJ/mol
η_i	effectiveness factor for reaction i
μ_j	viscosity of component j, Pa s
ν_{ij}	stoichiometric coefficient (reaction i, component j)
ρ_B	bed density, kg_{cat}/m^3
ρ_g	gas density, $kg/m_f{}^3$

controlled feed of oxygen can be obtained by means of a permoselective inorganic membrane, aiming to operate the reactor under milder autothermal conditions and high hydrocarbon conversion.

In the present contribution, a theoretical study of a multitubular membrane reactor for the autothermal reforming of methane over a $Ni/MgOAl_2O_3$ catalyst is presented. By means of a 1D pseudo-homogeneous model, the convenience of the proposed design to produce hydrogen to feed a PEM fuel cell of 10 kW_{th} is analyzed. The influence of the operating conditions on the reactor behavior is studied.

2. Mathematical model

A one-dimensional, pseudo-homogeneous, steady-state model was used to represent the ATR of methane in a multitubular packed-bed membrane reactor.

In the design proposed, the inert membrane tubes are filled with catalyst particles. A stream of methane, steam and eventually O_2 is fed by the tube side while a fraction of oxygen is distributed from the shell side through the tubular porous membrane (Fig. 1).

2.1. Model assumptions

To simulate the ATR membrane reactor, the following hypotheses have been assumed:

- axial mass and energy dispersions and external transport limitations are neglected because of the high total flowrates through the catalyst bed.
- internal mass transport limitations are accounted for by means of constant effectiveness factors for the four reactions under consideration [3].
- the catalyst particle is assumed to be isothermal.
- the use of tubes of small diameter (0.0156 m) supports the assumption of relatively flat mass and temperature radial profiles (1D model).

The reactor shell is assumed to be adiabatic, and isobaric conditions are selected for the oxygen flowing on the shell side. A cocurrent flow configuration is adopted. The friction factor f proposed by Ergun is employed to predict the pressure drop in the tubes.

The reactor model is represented by the following equations.

2.1.1. Reaction side (catalyst tubes)

Mass balances

$$\frac{dF_j}{dz} = A_T \rho_B \sum_{i=1}^{4} \nu_{ij} \eta_i r_i \quad j = CH_4,\ H_2O,\ CO_2,\ CO,\ H_2 \tag{1}$$

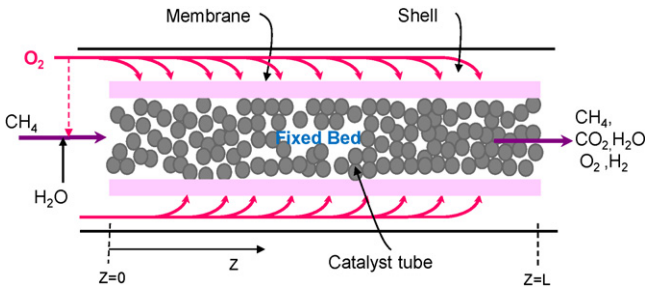

Fig. 1. Scheme of the simulated reactor for ATR of methane.

Table 1
Kinetic scheme and reaction rate expressions.

	Reaction	Kinetic expressions
1	$CH_4 + 2O_2 \rightarrow CO_2 + 2H_2O$	$r_1 = \frac{k_1{}^a p_{CH_4} p_{O_2}}{(1+K^{OX}_{CH_4} p_{CH_4} + K^{OX}_{O_2} p_{O_2})^2} + \frac{k_1{}^b p_{CH_4} p_{O_2}}{(1+K^{OX}_{CH_4} p_{CH_4} + K^{OX}_{O_2} p_{O_2})}$
2	$CH_4 + H_2O \leftrightarrow CO + 3H_2$	$r_2 = \frac{k_2/p^{2.5}_{H_2}(p_{CH_4} p_{H_2O} - p^3_{H_2} p_{CO}/K_{eq,2})}{(1+K_{CO} p_{CO} + K_{H_2} p_{H_2} + K_{CH_4} p_{CH_4} + K_{H_2O} p_{H_2O}/p_{H_2})^2}$
3	$CO + H_2O \leftrightarrow CO_2 + H_2$	$r_3 = \frac{k_3/p_{H_2}(p_{CO} p_{H_2O} - p_{H_2} p_{CO_2}/K_{eq,3})}{(1+K_{CO} p_{CO} + K_{H_2} p_{H_2} + K_{CH_4} p_{CH_4} + K_{H_2O} p_{H_2O}/p_{H_2})^2}$
4	$CH_4 + 2H_2O \leftrightarrow CO_2 + 4H_2$	$r_4 = \frac{k_4/p^{3.5}_{H_2}(p_{CH_4} p^2_{H_2O} - p^4_{H_2} p_{CO_2}/K_{eq,4})}{(1+K_{CO} p_{CO} + K_{H_2} p_{H_2} + K_{CH_4} p_{CH_4} + K_{H_2O} p_{H_2O}/p_{H_2})^2}$

$$\frac{dF_j}{dz} = A_T \rho_B \sum_{i=1}^{1} \nu_{ij} \eta_i r_i + J_j \pi d_T \quad j = O_2 \tag{2}$$

Energy balance

$$\frac{dT}{dz} = \frac{A_T}{\sum_{j=1}^{6} F_j Cp_j} \left[\rho_B \sum_{i=1}^{4} \eta_i r_i (-\Delta H_{r_i}) - \frac{4}{d_T} (J_{O_2} Cp_{O_2} + U)(T - T_S) \right]$$
$$j = CH_4,\ H_2O,\ CO_2,\ CO,\ H_2,\ O_2 \tag{3}$$

Momentum equation

$$\frac{dP}{dz} = -\frac{f \rho_g {u_s}^2}{d_p} \tag{4}$$

2.1.2. Permeation side (shell)

Mass balance

$$\frac{dF^S_j}{dz} = -J_j \pi d_T n_T \quad j = O_2 \tag{5}$$

Energy balance

$$\frac{dT_S}{dz} = \frac{U \pi d_T n_T (T - T_S)}{F_{O_2} Cp_{O_2}} \tag{6}$$

where the permeation flux is quantified by the following expression [10]:

$$J_j = -\frac{1}{RT_m} \left(\frac{D^e_j}{\delta} (p_j - p_{j,S}) + \frac{B_0}{\delta \mu_j} p_{j,S} (P - P_S) \right) \quad j = O_2 \tag{7}$$

$$D^e_j = \left(\frac{1}{D^e_{ij}} + \frac{1}{D^e_{j,k}} \right)^{-1} \tag{8}$$

$$D^e_{j,k} = K_0 \sqrt{\frac{8RT}{\pi M_j}} \tag{9}$$

Initial conditions

$$\text{At } z = 0: \quad F_j = F_{j0},\ F^S_j = F^S_{j0},\ T = T_0,\ T_S = T_{S0},\ P = P_0 \tag{10}$$

2.2. Kinetic model

The reaction scheme considered in the present contribution includes the complete combustion of methane, the steam reforming reactions and the WGSR [5,7,8]. The system of reactions and their kinetic expressions are shown in Table 1. The combustion of methane (reaction (1)) is evaluated by means of the kinetic model proposed by Trimm and Lam [11]. The steam reforming (reactions (2) and (4)) and WGS (reaction (3)) are assessed using the kinetics by Xu and Froment [1]. The equilibrium constants corresponding to reactions (2)–(4) of Table 1 were extracted from Elnashaie et al. [12].

Table 2
Geometrical parameters and operating conditions of the simulated membrane reactor.

Tube length, L	1 m
Internal tube diameter, d_T	0.0156 m
Shell diameter, d_S	0.3048 m
Number of tubes, n_T	109
Feed pressure, P_o	25 atm
Shell-side pressure, P_S	25–25.3 atm
Inlet tube temperature, T_0	535 °C
Inlet shell temperature, T_{S0}	535 °C
Total feed flowrate, F_{T0}	1,3136 kmol/h
Shell O_2 flowrate, F_{S0}	3 kmol/h
Catalyst	30% Ni/Al_2O_3
Catalyst diameter, d_p	0.001 m
Catalyst density, ρ_p	2355.3 kg/m^3
Space time, τ	3.36 kg_{cat}/(mol CH_4/min)
Membrane thickness, δ	0.00175 m
$F^0_{H_2O}/F^0_{CH_4}$	1.4 [4]
$F^T_{O_2}/F^0_{CH_4}$	0.598
$F^0_{H_2}/F^0_{CH_4}$	0.0003

Different effectiveness factors for the four reactions are considered. They are: $\eta_1 = 0.05$, $\eta_2 = 0.07$, $\eta_3 = 0.7$ and $\eta_4 = 0.06$ [3]. As suggested by De Groote and Froment [3], these values were considered constant along the reactor length.

2.3. Varying degree of reduction model (VDR)

An important problem in the modelling of the partial oxidation of methane is the degree of reduction of the Ni catalyst required for the steam reforming. According to the observations reported by Dissanayake et al. [13], the steam reforming would be consecutive to the complete combustion of CH_4. This has been accounted for in the present simulations by multiplying the rates of the steam reforming reactions and the WGS reaction by a *reduction factor*, which is a power function of the fractional oxygen conversion. This approach was called by De Groote and Froment [3] as *Varying Degree of Reduction Model* (*VDR*).

2.4. Additional considerations

The overall heat-transfer coefficient (U) is evaluated using the Crider and Foss equation [14]. The heat-transfer coefficient for the process gas side is calculated by means of the equation of Leva [15], and that corresponding to the shell side is calculated using the Delaware method [16].

In order to avoid the multiplicity of steady states inherent to countercurrent operation, a cocurrent flow configuration between the process gas and the coolant (O_2) streams is selected. Additionally, the cocurrent scheme lowers the hot spots, which leads to longer catalyst life, and reduces the parametric sensitivity, which ensures safe operating conditions [17].

It is considered that the reactor is cooled both by convective heat exchange between reactants and coolant and by cold-shot of oxygen permeated through the membrane (see Eq. (3)).

A commercial tubular microfiltration membrane (SCT, Inocermic) is selected for the simulations [18]. The membrane was modified by deposition of silica in order to attain the desired permeation characteristics. The parameters K_0 and B_0 (Eqs. (7) and (9)) were obtained from Pedernera et al. [19]. The geometric parameters of the reactor and the membrane, together with the operating conditions used in the simulations, are given in Table 2.

The diameter and density of the catalyst particles, as well as the bed porosity were extracted from [20].

The length and disposition of the tubes for the proposed design were adopted from the guidelines suggested by Kern for heat exchangers [21].

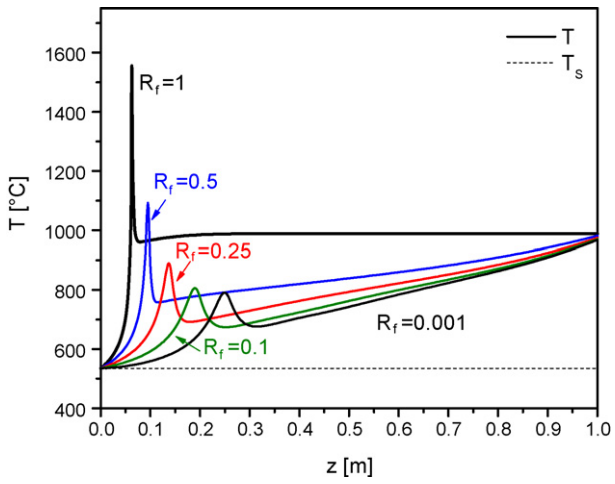

Fig. 2. Axial temperature profiles for different oxygen feed distribution ($R_f = F^0_{O_2}/F^T_{O_2}$) at constant total oxygen feed ($F^T_{O_2} = 5.87\,Nm^3/h$). Oxygen/methane feed ratio: $F^T_{O_2}/F^0_{CH_4} = 0.598$. Adiabatic operation.

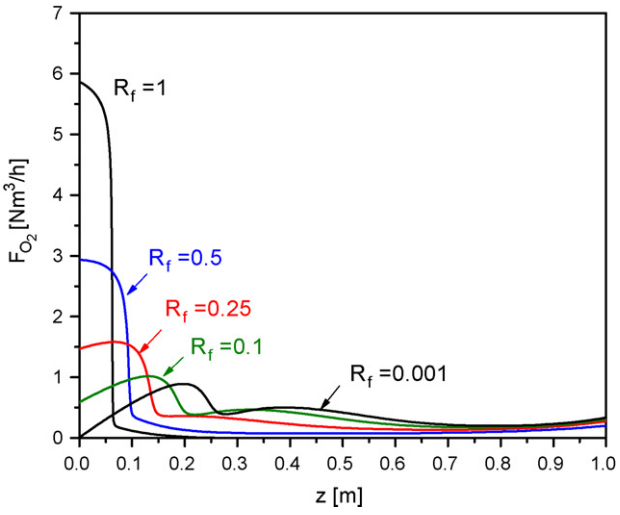

Fig. 3. Oxygen flowrate (F_{O_2}) along the reactor length for the conditions of Fig. 2.

The global selectivity (S_G) to hydrogen is calculated as the ratio between the amount of hydrogen produced and the amount of methane consumed, from the reactor inlet to the desired axial coordinate.

$$S_G = \frac{(F_{H_2} - F_{H_2,0})/\nu_{H_2}}{(F_{CH_4,0} - F_{CH_4})/\nu_{CH_4}} \quad (11)$$

Based on reaction (4), a value of 4 is adopted for the stoichiometric coefficient ν_{H_2}.

3. Results and discussion

3.1. Influence of the oxygen feed distribution

3.1.1. Adiabatic case

To analyze the influence of the oxygen feed distribution on the performance of the ATR reactor, a common basis of comparison is adopted: a constant total oxygen flowrate is fed to the reactor. As a first step in the present analysis, the overall heat-transfer coefficient between tube and shell sides is assumed to be zero. The remaining operating conditions are reported in Table 2.

Fig. 2 shows the temperature profiles along the reactor length for different oxygen feed distributions. The parameter R_f represents the ratio between the oxygen being fed at the reactor inlet ($F^0_{O_2}$) and the total oxygen feed ($F^T_{O_2}$); i.e., $R_f = F^0_{O_2}/F^T_{O_2}$. The pressure on the shell side is adjusted to modify the permeation rate through the membrane in order to keep constant the total feed of oxygen ($F^T_{O_2} = 5.869\,Nm^3/h$). When the permeation flow through the membrane is cancelled, all the O_2 is fed at the reactor mouth. This case corresponds to the conventional adiabatic fixed-bed reactor, represented by curve $R_f = 1$. As expected, a pronounced hot spot near the reactor inlet appears, as a consequence of the fast evolution of the combustion reaction. Probably, the value of the temperature peak will be lower in practice, because of the evolution of homogeneous steam reforming reactions. Further on the hot spot, the sharp temperature decrease indicates a predominance of the endothermic reforming reactions, because of the oxygen depletion. For axial positions $z > 0.20$ m, the temperature keeps almost constant at 988 °C.

When half of oxygen is fed through the membrane ($R_f = 0.5$) the hot spot is much less pronounced and shifts to the right. For lower values of R_f, this trend is confirmed and milder temperature profiles are observed. When almost all the O_2 is fed through the membrane (i.e., $R_f = 0.001$), the hot spot is below 800 °C and the maximum temperature is located at the outlet (970 °C).

Fig. 3 shows the oxygen flowrate along the catalyst tubes for the same conditions as Fig. 2. It is clear that the use of a membrane reactor prevents high concentrations of O_2 along the tube length. When most of the oxygen is fed trough the membrane ($R_f \leq 0.1$), it is possible to find operating conditions for which the rate of O_2 consumption by chemical reaction is nearly balanced with the rate of permeation through the membrane. As a result, very low O_2 concentrations are found in the catalyst bed and a reasonable degree of reduction of the catalyst leads to significant reforming reaction rates in a wider reactor zone. For the case of the conventional fixed-bed reactor ($R_f = 1$), the outlet conversion of O_2 is almost unitary. However, for the curves corresponding to the membrane reactor, a fraction of the permeated O_2 is not converted and a small O_2 slip is observed. This is clearly a non-desired situation that could be avoided by implementing a non-porous wall in the last section of the tubes, aiming to deplete the remaining O_2.

The results of Fig. 4 show that the outlet CH_4 conversion is high in all the cases (the reaction mixture is close to equilibrium), although the outlet conversions for the membrane reactor are slightly lower than that of $R_f = 1$, because the consumption of O_2 is not complete (see Fig. 3). For the same operating conditions,

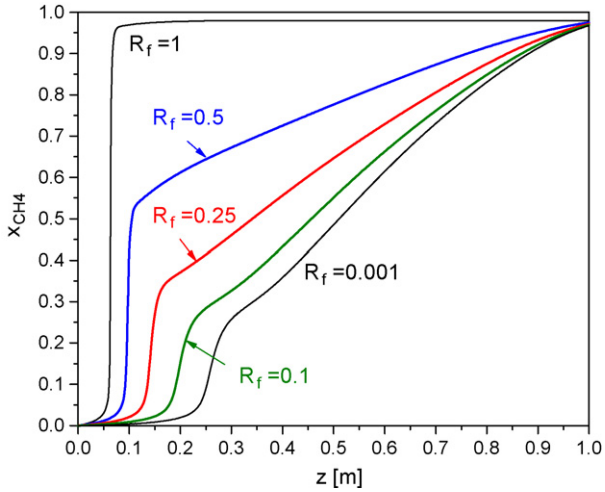

Fig. 4. Axial profiles of CH_4 conversion for the conditions of Fig. 2.

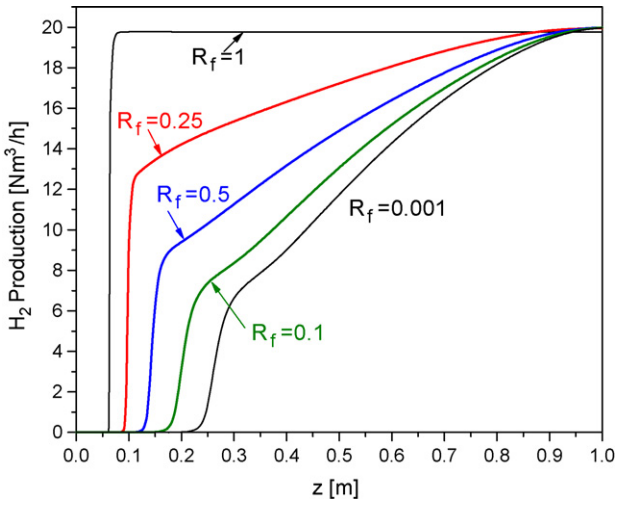

Fig. 5. Hydrogen flowrates along the tube length for the conditions of Fig. 2.

Fig. 5 shows the H_2 total flowrate along the reactor. When all the O_2 is fed to the reactor inlet ($R_f = 1$), a sudden increase in the conversion of CH_4 is observed at $z \approx 0.06$ m (see Fig. 4), which is associated to its consumption first by combustion (Fig. 3) and then by steam reforming, which leads to a fast hydrogen production (Fig. 5). As the parameter R_f decreases, the methane consumption and the H_2 production are more gradual along the reactor length. The results corresponding to $R_f = 0.001$ (all the O_2 is fed through the membrane) show that the hydrogen production starts beyond $z = 0.22$ m, at a reactor position where the O_2 concentration is low enough to allow the simultaneous occurrence of the combustion and reforming reactions. For axial positions $z > 0.30$ m, the heat generation by combustion exceeds the heat consumption by steam reforming. The existence of combustion for $z > 0.30$ is confirmed by inspection of Fig. 2, where a continuous increase in temperature is verified. The coexistence with steam reforming is confirmed in Fig. 5, where a gradual increase in the H_2 production is observed. It is important to note that the outlet H_2 production is slightly higher for the membrane reactor than for the conventional reactor (Fig. 5), despite the fact that the outlet CH_4 conversion is the opposite (Fig. 4). This result can be explained by a slightly higher selectivity to H_2.

3.1.2. Non-adiabatic case

The previous assumption of adiabatic conditions ($U = 0$) is suitable for a first analysis of the thermal effects associated to ATR in a membrane reactor. In practice, however, a certain amount of the generated heat is transferred to the fluid being circulated through the shell. To represent this, some of the previous results are compared with those corresponding to non-adiabatic membranes. The overall heat-transfer coefficient (U) is calculated as stated in Section 2.

Fig. 6 shows the temperature profiles of two conditions of Fig. 2 ($R_f = 1$ and $R_f = 0.001$, for $U = 0$), which are compared with those corresponding to the non-adiabatic case (curves for the shell-side temperature T_S are also included).

When $R_f = 1$, the existence of a cooling medium leads to a lower hot spot. The difference between both hot spots is not important, because the heat generation by methane combustion is concentrated in a narrow zone of the catalyst bed (around $z = 0.06$ m). In this very short section of the tubes, the heat transfer to the shell side is limited by the low heat-transfer area. Nevertheless, for the calculated average U values (close to 20 W/m^2 K), the outlet temperature for the non-adiabatic case is approximately 160 °C lower than that of the adiabatic operation. For the membrane reactor ($R_f = 0.001$), the decrease in the outlet temperature is around

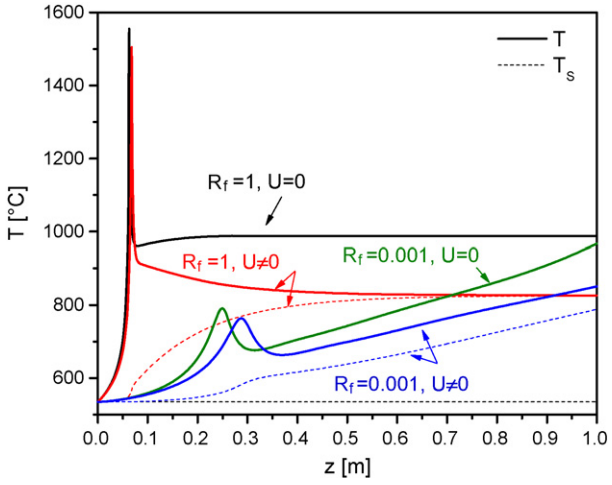

Fig. 6. Axial temperature profiles for conventional ($R_f = 1$) and membrane ($R_f = 0.001$) reactors, operating under adiabatic ($U = 0$) and non-adiabatic conditions ($U \neq 0$). Constant total oxygen feed ($F^T_{O_2} = 5.87$ N m^3/h).

115 °C due to the convective heat transfer. The most important point to remark is that the maximum temperature for the membrane reactor (at $z = 1$ m) is considerably lower than the hot-spot temperature for the conventional fixed-bed reactor for analogous operating conditions.

The hydrogen production rates for adiabatic and non-adiabatic conditions are compared in Fig. 7. For $R_f = 1$ and $U \neq 0$, the continuous temperature decrease beyond the hot-spot causes the reversal of the steam reforming reactions (methanation). This phenomenon is favoured by the low partial pressures of CH_4 and high partial pressures of H_2 (see the kinetic expressions for reactions (2) and (4), Table 1). As a consequence, the outlet H_2 production diminishes with respect to the adiabatic case. Conversely, for the curves corresponding to $R_f = 0.5$ and 0.001 the reversal phenomenon does not appear. The cooling effects are also present, which deteriorates the outlet production rate with respect to the adiabatic conditions. However, the lateral feed of oxygen leads to a continuous temperature increase and a more gradual methane conversion. Indeed, the membrane reactor presents a continuous increase in the H_2 flowrate along the tube length and slightly higher H_2 productions than that of the fixed-bed reactor.

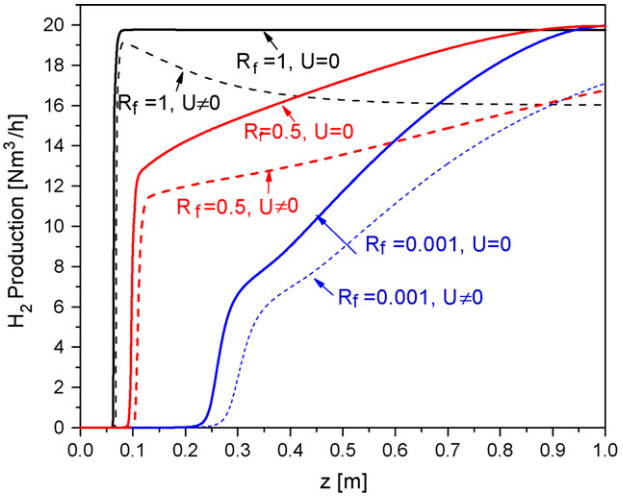

Fig. 7. Hydrogen flowrates along the tube length for three different oxygen feed distributions ($R_f = 1$, 0.5 and 0.001): comparison between adiabatic and non-adiabatic operations.

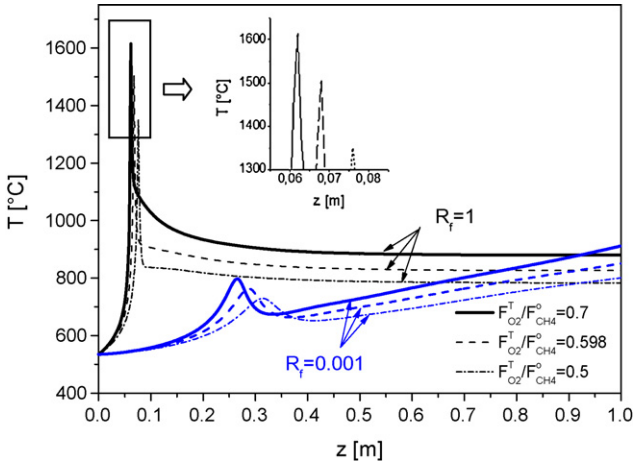

Fig. 8. Axial temperature profiles for the two extreme oxygen feed distributions ($R_f = 0.001$ and $R_f = 1$), at three different $F^T_{O_2}/F^0_{CH_4}$ ratios.

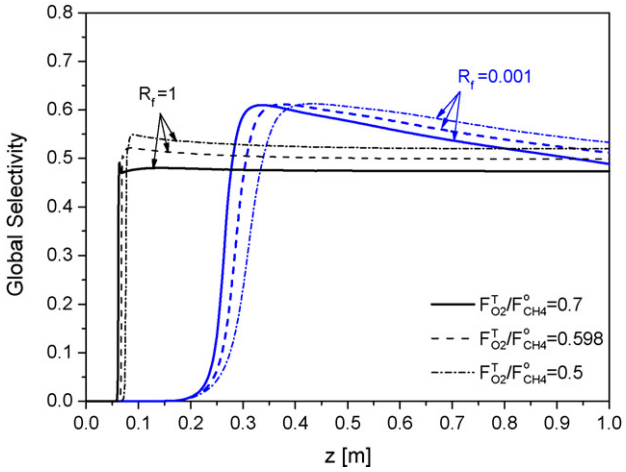

Fig. 10. Axial profiles of global selectivity to H_2 (S_G) for the conditions of Fig. 8.

3.2. Influence of the $F^T_{O_2}/F^0_{CH_4}$ ratio

The influence of the $F^T_{O_2}/F^0_{CH_4}$ ratio on the operation of the ATR reactor is discussed for two extreme oxygen feed distributions: $R_f = 1$ (conventional reactor) and $R_f = 0.001$ (membrane reactor). The non-adiabatic case is considered. The parameters used in the simulations are given in Table 2.

The temperature profiles for three $F^T_{O_2}/F^0_{CH_4}$ ratios are included in Fig. 8. The results were obtained by assuming constant feed flowrates of CH_4 (9.81 Nm^3/h) and H_2O (13.74 Nm^3/h). As before, the specified feed ratios ($F^T_{O_2}/F^0_{CH_4} = 0.5$, 0.598 and 0.7) for the membrane reactor were obtained by setting the pressure on the shell side.

As expected, for both reactor designs the temperature increases as the O_2 feed is higher. However, the values of the maximum temperatures corresponding to the membrane reactor (800, 850, 910 °C, at $z = 1$ m) are considerably lower than those of the conventional reactor (1350, 1500, 1615 °C, at $z \approx 0.06$–0.08 m). These results suggest that the $F^T_{O_2}/F^0_{CH_4}$ ratio could be increased for the case $R_f = 0.001$, if it were convenient to optimize the H_2 production rate.

Fig. 9 shows the conversion of CH_4 along the tube length for the same conditions as Fig. 8. The membrane reactor shows outlet conversions slightly higher for the three feed ratios, due to the phenomenon of reversal of reactions (2)–(4) caused by the coolant in the case $R_f = 1$, as discussed in the previous section. Regarding the selectivity to H_2 (Eq. (11)), it is interesting to note that the outlet selectivity for $R_f = 0.001$ exceeds the one corresponding to the conventional reactor, for the three studied feed ratios (Fig. 10). As a result of the higher CH_4 conversion and selectivity, the membrane reactor presents a H_2 production rate between 4.8% and 6.5% over that of the conventional reactor. For the analyzed range of operating conditions, the H_2 production rate for both designs increases with $F^T_{O_2}/F^0_{CH_4}$. Fig. 10 also shows that the selectivity to H_2 diminishes with the $F^T_{O_2}/F^0_{CH_4}$ ratio, because at higher temperatures the equilibrium of the Water Gas Shift Reaction is shifted to the left. This result suggests the existence of an optimal value of the $F^T_{O_2}/F^0_{CH_4}$ ratio, which maximizes the H_2 production rate. For adiabatic fixed-bed ATR reactors it is well known that there is an optimum value for the oxygen feed, a point that has been discussed widely [4,5,22,23]. For the case of a membrane ATR reactor, the optimum value for the oxygen feed ratio is determined not only by production reasons, but also by safety reasons. Indeed, if the value $F^T_{O_2}/F^0_{CH_4}$ becomes too high, the risk associated to the O_2 slip tends to increase. This is confirmed in Fig. 11, which shows that the outlet O_2 flowrate increases for higher values of the oxygen feed ratio.

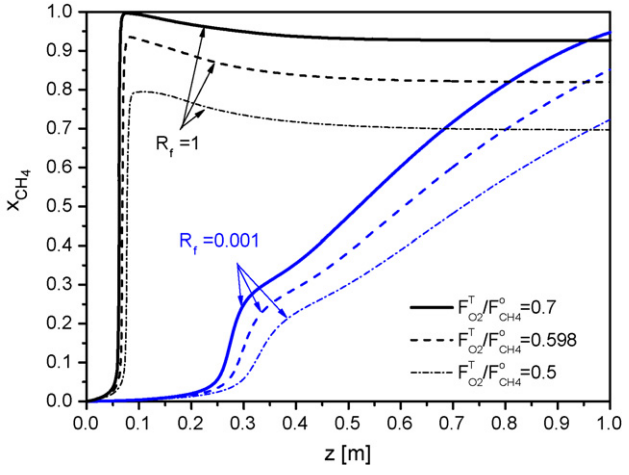

Fig. 9. Axial profiles of CH_4 conversion for the conditions of Fig. 8.

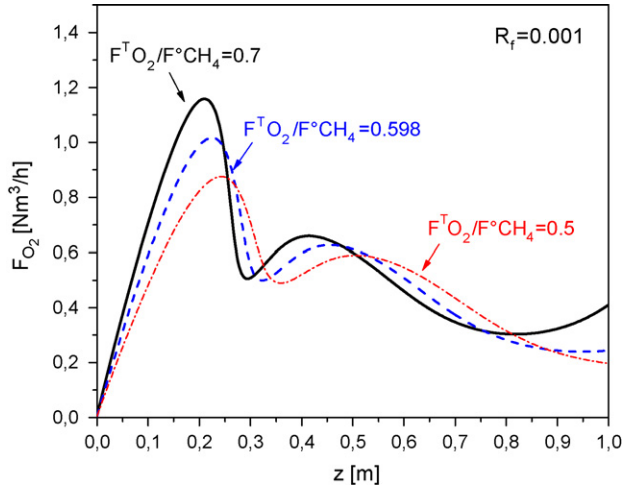

Fig. 11. Oxygen flow rate (F_{O_2}) along the reactor length for the ATR membrane reactor ($R_f = 0.001$) for the conditions of Fig. 8.

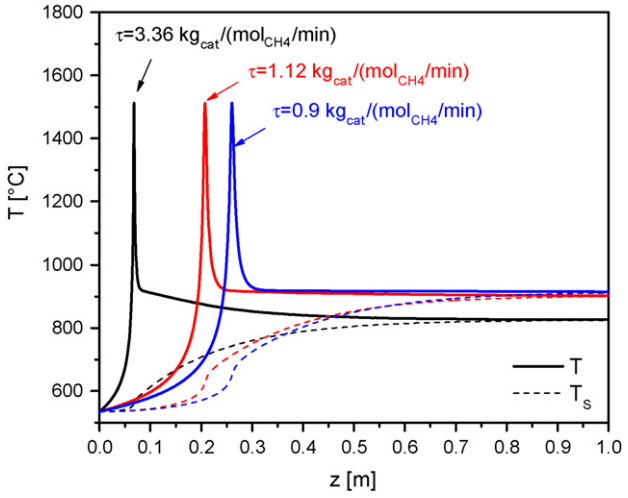

Fig. 12. Axial temperature profiles for different space times (τ) at constant feed ratios: $F^0_{H_2O}/F^0_{CH_4} = 1.4$, $F^T_{O_2}/F^0_{CH_4} = 0.598$, $F^0_{H_2}/F^0_{CH_4} = 0.0003$. R_f=1. Non-adiabatic operation.

3.3. Influence of the space time

To analyze the influence of the space time (τ), the methane flowrate is increased from its reference value ($F^0_{CH_4}$ = 0.438 kmol/h). All the feed ratios ($F^0_{H_2O}/F^0_{CH_4}$; $F^T_{O_2}/F^0_{CH_4}$; $F^0_{H_2}/F^0_{CH_4}$) are kept constant at the values reported in Table 2.

Fig. 12 shows the effect of the space time on the axial temperature profiles when all the oxygen is fed at the reactor inlet (R_f = 1). As the space time is decreased, the value of the maximum temperature is not modified significantly, even though the axial location of the hot spot shifts to the outlet. The outlet temperature, however, increases as the total flowrate is higher, as a consequence of the different heat-transfer rates to the shell side. For the case R_f = 0.001, the space time strongly affects the hot spots (Fig. 13). As τ decreases, the hot spot increases from 768 to 1165 °C and its location moves to the right. This phenomenon is a consequence of the higher oxygen permeation rates through the membrane to keep constant the feed ratio at $F^T_{O_2}/F^0_{CH_4} = 0.598$. These higher O_2 fluxes lead to an accumulation of oxygen inside the tubes (upper Fig. 14), which causes the catalyst not to reach the degree of reduction required for the

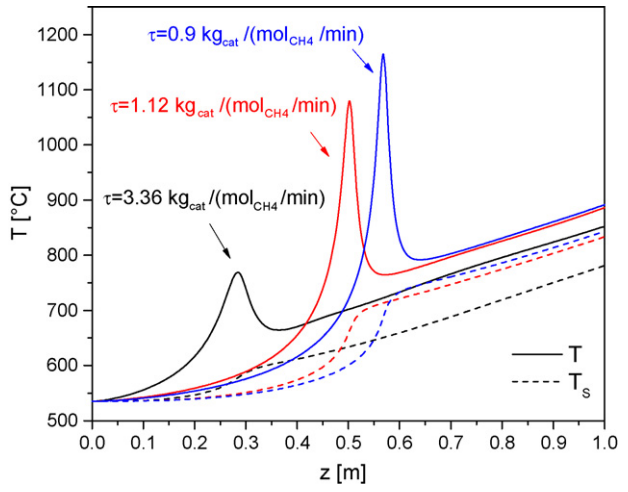

Fig. 13. Axial temperature profiles for different space times (τ) at constant feed ratios: $F^0_{H_2O}/F^0_{CH_4} = 1.4$, $F^T_{O_2}/F^0_{CH_4} = 0.598$, $F^0_{H_2}/F^0_{CH_4} = 0.0003$. R_f = 0.001. Non-adiabatic operation.

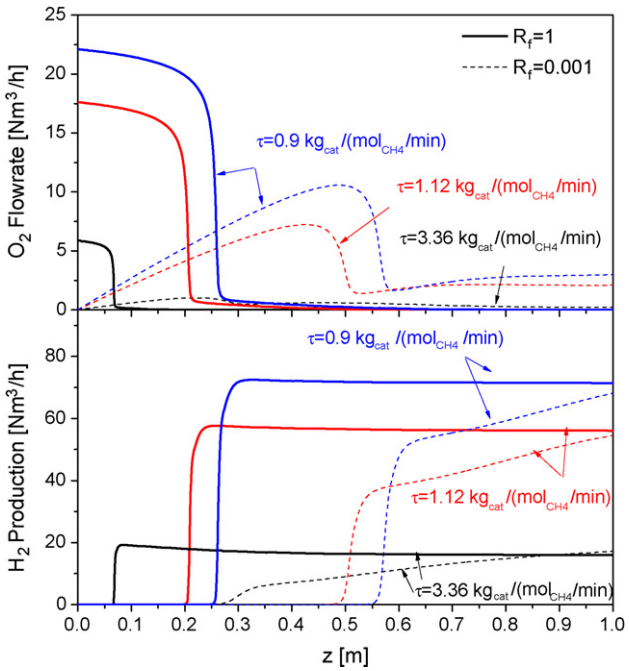

Fig. 14. Oxygen flowrate (F_{O_2}) and H_2 production along the reactor length for the conditions of Figs. 12 and 13.

endothermic steam reforming reactions. Therefore, the combustion reaction becomes predominant and higher temperature peaks appear. However, it is important to note that even in the worst case (τ = 0.9 $kg_{cat}/mol_{CH_4}/min$) the hot spot corresponding to R_f = 0.001 is considerably lower than those of R_f = 1 (compare Figs. 12 and 13). Fig. 14 also shows the variation in the H_2 production resulting from the increase in the CH_4 feed.

4. Conclusions

The results presented in the previous sections lead to the following conclusions:

- the autothermal reforming of methane could be carried out in a membrane reactor, provided that an appropriate amount of O_2 is fed through the membrane pores.
- for comparable hydrogen production rates, the distribution of the oxygen feed by means of the membrane leads to lower O_2 concentrations in the reaction mixture and less severe thermal conditions. This milder temperature profiles can extend considerably the catalyst life and reduce the thermal stress on the reactor materials.
- from the standpoint of the thermal stress and catalyst stability, it is clear that the membrane reactor offers more flexibility to define the amount of O_2 to be fed.
- the membrane reactor would make it possible to produce H_2 in a better distributed way along the reactor length, with continuous consumption of O_2 by combustion and coexistence of exothermic and endothermic reactions, because of a reasonable degree of reduction of the Ni catalyst.

The possible failure of a membrane tube is a safety problem that should be analyzed carefully, in order to avoid conditions of reactor runaway and/or the formation of explosive mixtures.

References

[1] J. Xu, G.F. Froment, AIChE J. 35 (1989) 88.
[2] T. Numaguchi, K. Kikuchi, Chem. Eng. Sci. 43 (1988) 2295.

[3] A.M. De Groote, G.F. Froment, Appl. Cat. A: Gen. 138 (1996) 245.
[4] K. Aasberg-Petersen, J. Bak-Hansen, T. Christensen, I. Dybkjaer, P. Seier Christensen, C. Stub Nielsen, S. Winter Madsen, J. Rostrup-Nielsen, Appl. Cat. A: Gen. 221 (2001) 379.
[5] T. Christensen, P. Christensen, I. Dybkjaer, J. Bak-Hansen, I. Primdahl, Developments in autothermal reforming, Stud. Surf. Sci. Catal. 119 (1998) 883.
[6] J. Hüppmeier, M. Baune, J. Thöming, Chem. Eng. J. 142 (2008) 225.
[7] T.P. Tiemersma, C.S. Patil, M. van Sint Annaland, J.A.M. Kuipers, Chem. Eng. Sci. 61 (2006) 1602.
[8] C.R.H. De Smet, M.H.J.M. de Croon, R.J. Berger, G.B. Marin, J.C. Schouten, Chem. Eng. Sci. 56 (2001) 4849.
[9] V.L. Barrio, G. Schaub, M. Rohde, S. Rabe, F. Vogel, J.F. Cambra, P.L. Arias, M.B. Güemez, Int. J. Hydrogen Energy 32 (2007) 1421.
[10] R. Mallada, Ph.D. Thesis, University of Zaragoza, Spain (1999).
[11] D.L. Trimm, C.W. Lam, Chem. Eng. Sci. 35 (1980) 1405.
[12] S.S.E.H. Elnashaie, S.S. Elshishini, Modeling, Simulation and Optimization of Industrial Fixed Bed Catalytic Reactors, Gordon and Breach Science, Switzerland, 1993.
[13] D. Dissanayake, M.P. Rosynek, K.C.C. Kharas, J.H. Lunsford, J. Catal. 132 (1991) 117.
[14] J.E. Crider, A.S. Foss, AIChE J. 11 (1965) 1012.
[15] G.F. Froment, K.B. Bischoff, Chemical Reactor Analysis and Design, Wiley, Canada, 1990.
[16] R.W. Serth, Process Heat Transfer. Principles and Applications, Elsevier Science, 2007.
[17] D.O. Borio, J.E. Gatica, J.A. Porras, AIChE J. 35 (1989) 287.
[18] R. Mallada, M. Pedernera, M. Menéndez, J. Santamaría, Ind. Eng. Chem. Res. 39 (2000) 620.
[19] M. Pedernera, R. Mallada, M. Menéndez, J. Santamaría, AIChE J. 46 (2000) 2489.
[20] M.N. Pedernera, J. Piña, D.O. Borio, Chem. Eng. J. 134 (2007) 138.
[21] D.Q. Kern, Procesos de Transferencia de Calor, Compañía Edit. Cont., México, 1997.
[22] T. Christensen, I. Primdahl, Improve syngas production using autothermal reforming, Hydrocabon Process. March (1994).
[23] J. Piña, D.O. Borio, Lat. Am. Appl. Res. 36 (2006) 289.